Contribution from the Laboratoire de Spectrochimie des Elements de Transition, UA 420, and Institut d'Electronique Fondamentale, UA 022, Université de Paris Sud, 91405 Orsay, France, Department of Chemistry, University of Bergen, 5007 Bergen, Norway, and Laboratoire de Chimie du Solide, LP 8661, Université de Bordeaux 1, 33405 Talence, France

Structure and Magnetism of the First Alternating Bimetallic Chain Compound $MnCu(obp)(H_2O)_3 \cdot H_2O$ (opb = Oxamidobis(propionato))

Yu Pei,[1a] Olivier Kahn,*[1a] Jorunn Sletten,[1b] Jean-Pierre Renard,[1c] Roland Georges,[1d] Jean-Claude Gianduzzo,[1d] Jacques Curely,[1d] and Qiang Xu[1d]

Received July 16, 1987

The title compound has been synthesized and its crystal structure at 92 K has been determined. The compound crystallizes in the triclinic system, space group $P\bar{1}$, with $a = 8.538$ (2) Å, $b = 9.248$ (8) Å, $c = 10.687$ (3) Å, $\alpha = 67.73$ (5)°, $\beta = 63.28$ (2)°, $\gamma = 74.08$ (5)°, and $Z = 2$ (MnCu units). The structure consists of centrosymmetrically related double chains with octahedral Mn^{II} and square-pyramidal Cu^{II} bridged by oxamido (Mn···Cu = 5.452 Å) and carboxylato (Mn···Cu = 6.066 Å) groups. The magnetic interactions between adjacent Mn^{II} and Cu^{II} within a single chain are much larger than the interaction between two symmetry-related Cu^{II} atoms through a long apical Cu–O (2.625 Å) bond, so that magnetically the compound behaves as an alternating bimetallic chain. The magnetic susceptibility has been studied in the $1.5 \text{ K} < T < 300$ K temperature range. The $\chi_M T$ versus T plot, χ_M being the molar magnetic susceptibility per MnCu unit, exhibits a minimum at about 40 K and a sharp maximum at 2.9 K, which is characteristic of bimetallic chains with antiferromagnetic intrachain interactions and very weak antiferromagnetic interchain interaction. The three-dimensional antiferromagnetic long-range order occurs at 2.31 (2) K. A theoretical model has been developed to interpret quantitatively the magnetic data. $S_{Mn} = {}^5/_2$ has been taken as a classical spin and $S_{Cu} = {}^1/_2$ as a quantum spin, and the intrachain interactions have been assumed to be purely isotropic. The interaction parameters have been found as J_1 (through oxamido) = −32.0 (7) cm^{-1} and J_2 (through carboxylato) = −6.8 (7) cm^{-1} (the exchange Hamiltonian for a pair being written $-J_{ij}\vec{S}_i \cdot \vec{S}_j$). The mechanism of the intrachain as well as interchain interactions has been discussed.

Introduction

One-dimensional magnetism is a field where the breakthroughs in theory and in design of new classes of compounds have mutually stimulated each other.[2-4] To sum up in a few words the history of this field, we can say that, at first, the studied compounds were regular homometallic chains, in which the magnetic centers are equally spaced along the chain.[5-8] Then, about a decade ago, alternating homometallic chains appeared, in which there are two intrachain exchange parameters.[2,9-12] The interest for compounds of this kind was largely due to their relevance to the problem of the spin Peierls distorsion.[13,14] More recently, the first regular bimetallic chains were described,[15-20] and new theoretical models adapted to these systems were formulated.[21-25] These novel one-dimensional compounds are particularly attractive, in particular because whatever the nature of the interaction between nearest neighbors may be, they exhibit a ferromagnetic-like behavior in the low-temperature range;[26] $\chi_M T$ diverges when T approaches zero, χ_M being the molar magnetic susceptibility per bimetallic unit and T the temperature. When the intrachain interaction is antiferromagnetic, the $\chi_M T$ versus T plot exhibits a characteristic minimum, which may be considered as the signature of one-dimensional ferrimagnetic behavior. The magnetic properties in the very low-temperature range are influenced by the interchain interactions, which can never be totally ignored. In most of the cases, these interchain interactions lead to the onset of a three-dimensional antiferromagnetic ordering, with a sharp maximum of $\chi_M T$ (and χ_M).[16-19] In one case,[20] so far, it has been possible to assemble the ferromagnetic chains within the crystal lattice in a ferromagnetic fashion, so that the compound presents a spontaneous magnetization below a critical temperature of 4.6 K.

Since the possibilities of synthesis in molecular chemistry are (almost) limitless, it was foreseeable that shortly after the alternating homometallic chains and the regular bimetallic chains, the first alternating bimetallic chain would be reported. This report is made in this paper.

In the following sections, we successively describe the synthesis of $MnCu(obp)(H_2O)_3 \cdot H_2O$, where obp is the ligand oxamido-

(1) (a) Laboratoire de Spectrochimie des Elements de Transitiion, Université de Paris Sud. (b) University of Bergen. (c) Institut d'-Electronique Fondamentale, Université de Paris Sud. (d) Université de Bordeaux 1.
(2) Landee, C. P. In *Organic and Inorganic Low Dimensional Crystalline Materials*; Delhaes, P., Drillon, M., Eds.; NATO Advanced Research Workshop; Plenum: New York; in press.
(3) de Jongh, L. J.; Miedema, A. R. *Adv. Phys.* **1974**, *23*, 1.
(4) Willett, R. D.; Gatteschi, D.; Kahn, O. *Magneto-Structural Correlations in Exchange Coupled Systems*; NATO ASI Series *C* 140; Reidel, Dordrecht, 1985.
(5) See: de Jongh, L. J.; Bonner, J. C.; Renard, J. P. in ref 4.
(6) Willett, R. D.; Gaura, R. M.; Landee, C. P. In *Extended Linear Chain Compounds*; Miller, J. S., Ed.; Plenum: New York, 1983; Vol. 3, p 143.
(7) Hatfield, W. E.; Estes, W. E.; Marsh, W. E.; Pickens, M. W.; Ten Haar, L. W.; Weller, R. W. In *Extended Linear Chain Compounds*; Miller, J. S., Ed.; Plenum: New York, 1983; Vol. 3, p 43.
(8) Renard, J. P.; Clement, S.; Verdaguer, M. *Proc.—Indian Acad. Sci., Chem. Sci.* **1987**, *98*, 131.
(9) See: Hatfield, W. E. in ref 4.
(10) Wolthuis, A. J.; Huiskamp, W. J.; de Jongh, L. J.; Reedijk, J. *Physica B+C* **1985**, *133B+C*, 161.
(11) Olmstead, M. M.; Musker, W. K.; Ten Haar, L. W.; Hatfield, W. E. *J. Am. Chem. Soc.* **1982**, *104*, 6627.
(12) Daoud, A.; Ben Salah, A.; Chappert, C.; Renard, J. P.; Cheikh-Rouhou, A.; Duc, T.; Verdaguer, M. *Phys. Rev. B: Condens. Matter* **1986**, *33*, 6253.
(13) Bray, J. W.; Interrante, L. V.; Jacobs, I. S.; Bonner, J. C. In *Extended Linear Chain Components*; Miller, J. S., Ed.; Plenum: New York, 1982; Vol. 3, p 353.
(14) de Jongh, L. J. In *Recent Developments in Condensed Matter Physics*; Devreese, J. J., Ed.; Plenum: New York, 1981; Vol. 1, p 343.
(15) Gleizes, A.; Verdaguer, M. *J. Am. Chem. Soc.* **1981**, *103*, 7373; **1984**, *106*, 3727.
(16) Beltran, D.; Escriva, E.; Drillon, M. *J. Chem. Soc., Faraday Trans. 2* **1982**, *78*, 1773.
(17) Drillon, M.; Coronado, E.; Beltran, D.; Curely, J.; Georges, R.; Nugteren, P. R.; de Jongh, L. J.; Genicon, J. L. *J. Magn. Magn. Mater.* **1986**, *54-57*, 1507.
(18) Pei, Y.; Sletten, J.; Kahn, O. *J. Am. Chem. Soc.* **1986**, *108*, 3143.
(19) Pei, Y.; Verdaguer, M.; Kahn, O.; Sletten, J.; Renard, J. P. *Inorg. Chem.* **1987**, *26*, 138.
(20) Pei, Y.; Sletten, J.; Kahn, O.; Sletten, J.; Renard, J. P. *J. Am. Chem. Soc.* **1986**, *108*, 7428.
(21) Drillon, M.; Coronado, E.; Beltran, D.; Georges, R. *Chem. Phys.* **1983**, *79*, 449.
(22) Verdaguer, M.; Julve, M.; Michalowicz, A.; Kahn, O. *Inorg. Chem.* **1983**, *22*, 2624.
(23) Verdaguer, M.; Gleizes, A.; Renard, J. P.; Seiden, J. *Phys. Rev. B: Condens. Matter* **1984**, *29*, 5144.
(24) Curely, J.; Georges, R.; Drillon, M. *Phys. Rev. B: Condens. Matter* **1986**, *33*, 6243.
(25) Georges, R.; Curely, J.; Drillon, M. *J. Appl. Phys.* **1985**, *58*, 914.
(26) Kahn, O. *Proc.—Indian Acad. Sci., Chem. Sci.* **1987**, *98*, 33.

0020-1669/88/1327-0047$01.50/0 © 1988 American Chemical Society

bis(propionato) derived from H_4opb, its crystal structure, and its

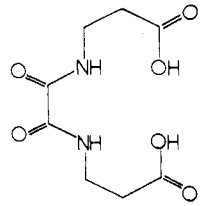

H_4opb

magnetic properties. We also present the broad outlines of a mathematical model appropriate to describe the magnetic properties of such an alternating bimetallic chain, and we determine the values of the two Mn^{II}–Cu^{II} intrachain exchange parameters through the oxamido and the carboxylato bridge, respectively.

Experimental Section

Synthesis. $MnCu(obp)(H_2O)_3 \cdot H_2O$ was synthesized in three steps. First, the organic compound oxamidobis(propionic acid), H_4obp, was prepared as follows: A solution of 10 mmol of diethyl oxalate in 15 mL of ethanol was added to a solution of 20 mmol of β-alanine and 20 mmol of NaOH in 10 mL of water. The mixture was heated at 60 °C for 4 h. A drop of concentrated hydrochloric acid was then added, and H_4obp precipitated as a polycrystalline powder. H_4obp was filtered, washed with ethanol, and dried under vacuum. The second step consisted of synthesizing the copper(II) mononuclear brick $Na_2[Cu(obp)] \cdot 3.5H_2O$. For that, 5 mmol of H_4opb and 20 mmol of NaOH were dissolved in 50 mL of water. A solution of 5 mmol of $Cu(NO_3)_2 \cdot 3H_2O$ in 10 mL of water was then added. The resulting solution was filtered and reduced to 10 mL by evaporation. Addition of ethanol afforded violet crystals of $Na_2[Cu(obp)] \cdot 3.5H_2O$. Finally, $MnCu(obp)(H_2O)_3 \cdot H_2O$ was obtained as well-shaped dark blue single crystals by slow evaporation of a solution of 2 mmol of $Na_2[Cu(obp)] \cdot 3.5H_2O$ and 2 mmol of $Mn(NO_3)_2 \cdot 4H_2O$ in 20 mL of water. Anal. Calcd for $C_8H_{16}N_2O_{10}CuMn$: C, 22.95; H, 3.85; N, 6.69; Cu, 15.18; Mn, 13.12. Found: C, 23.19; H, 3.61; N, 6.43; Cu, 14.96; Mn, 13.60.

Crystallographic Data Collection and Structure Determination. Information concerning conditions for crystallographic data collection and structure refinement is summarized in Table I. A light blue prismatic crystal was mounted and used for all data collection. Cell dimensions were determined from 16 reflections with θ angles between 10 and 20°. Intensity data were collected from one hemisphere. Three reference reflections were monitored and showed no significant deterioration.

The intensity distribution suggested a centrosymmetric space group; this was confirmed by the solution and refinement of the structure. Cu and Mn positions were derived from a Patterson map. The remaining non-hydrogen atoms were located in two subsequent Fourier maps. After anisotropic refinement, hydrogen atoms were located in a difference Fourier map and were refined with isotropic thermal parameters. In the final least-squares cycles, an extinction parameter was included. The refinement converged at $R = 0.028$, $R_w = 0.031$, and $s = 1.47$. Final atomic parameters for all atoms are listed in Table II. Anisotropic thermal parameters are listed in Table SI (supplementary material).

Magnetic Measurements. In the 3–300 K temperature range, these were carried out with a Faraday type magnetometer equipped with a helium continuous-flow cryostat. $HgCo(NCS)_4$ was used as a susceptibility standard. Diamagnetic correction was taken as -180×10^{-6} cm^3 mol^{-1}. In the 1.7–4.2 K range, the magnetic susceptibility was measured with a laboratory-made low-field SQUID magnetometer.

Description of the Structure

The compound forms bimetallic centrosymmetrically related double chains running in the [10$\bar{1}$] direction. A part of a chain is depicted in Figure 1, and the double chain is shown in Figure 2. Bond lengths and angles involving non-hydrogen atoms are given in Tables III and IV, respectively.

The Mn atom has somewhat distorted octahedral surroundings with two oxamido oxygen atoms, one carboxylato oxygen atom and one water molecule in equatorial positions. The equatorial atoms deviate significantly from planarity (–0.172, 0.208, –0.193, and 0.158 Å for O6[b], O1, O2, and O9, respectively), the Mn atom being close to the best plane through these atoms (–0.013 Å). The Cu atom is in distorted-square-pyramidal surroundings with two oxamido nitrogen atoms and two carboxylato oxygen atoms in equatorial positions, the apical position being occupied by a carboxylato oxygen atom from the centrosymmetrically related chain with a Cu[a]···O5 apical bond length of 2.625 (1) Å. This atom thus bridges two parallel chains, making up the double chain depicted in Figure 2. N1, N2, O3, and O4 deviate from the equatorial plane by –0.082, 0.081, 0.076 and –0.075 Å, respectively. The Cu atom is displaced 0.114 Å from this plane toward the apical position. The dihedral angle between the equatorial planes of Mn and Cu is 15.6°.

Within a single chain, the Mn and Cu atoms are bridged by an oxamido group O1O2C1C2N1N2 with a Mn···Cu separation of 5.452 (2) Å on the one hand and by a carboxylato group O4C8O6 with a Mn···Cu separation of 6.066 (2) Å on the other hand. The oxamido bridge is approximately planar (maximum deviation 0.04 Å), and makes a dihedral angle of 26.2° with the carboxylato bridge. The metal atoms deviate significantly from the planes of both bridges; the deviations from the oxamido plane are 0.20 and –0.08 Å for Mn and Cu, respectively, and, from the carboxylato plane, 0.24 and 0.35 Å.

Within the double chain, the Cu···Cu[a] separation is 5.118 (2) Å. The shortest metal···metal separations occur between neighboring double chains, Cu···Cu($-x$, $-y$, $1 - z$) being 4.262 (2) Å and Mn···Mn ($1 - x$, $-y$, $-z$) being 4.819 (2) Å. Both of these contacts are between double chains displaced by one unit cell in the y direction. A Mn···Mn ($-x$, $-y$, $-z$) distance of 5.118 (2) Å occurs between double chains in neighboring stacks. Double chains related by unit translations in the y direction as well as in the $x + y$ direction are laced together through hydrogen bonding. A list of hydrogen bonds is given in Table V.

Table I. Information Concerning the Crystallographic Data Collection and Refinement Conditions for $MnCu(obp)(H_2O)_3 \cdot H_2O$[a]

molecular formula	$CuMnC_8H_{16}N_2O_{10}$
fw	418.70
space group	$P\bar{1}$
temp at cryst, K	92
unit cell	
a, Å	8.538 (2)
b, Å	9.248 (8)
c, Å	10.687 (3)
V, Å^3	691.9 (9)
α, deg	67.73 (5)
β, deg	63.28 (2)
γ, deg	74.08 (5)
Z	2
D_{obsd} g cm^{-3}	2.009
μ(Mo Kα), cm^{-1}	24.71
range of transmissn factors	0.85–0.71
crystal size, mm	0.28 × 0.17 × 0.064
instrument	CAD-4
scan type	ω
scan range ($\Delta\omega$), deg	1.0 + 0.35 tan θ
scan speed deg/min	10
radiation	monochromated Mo Kα (λ = 0.71073 Å)
max 2θ, deg	56
no. of reflcns measd	2948
no. of obsd reflcns (NO)	2550
limit of obsd reflcns	$F_o > 2\sigma$
no. variables refined (NV)	263
extinction coeff	2.96×10^{-7}
agreement factors	
R	0.028
R_w	0.031
s	1.47

[a] Agreement factors are defined as follows: $R = \sum||F_o| - |F_c||\sum|F_o|$; $R_w = [\sum w(|F_o| - |F_c|)^2/\sum w|F_o|^2]^{1/2}$; $s = [\sum w(|F_o| - |F_c|)^2/(NO - NV)]^{1/2}$. The weighting scheme is defined by: $w = 1/\sigma_F^2$; $\sigma_F = \sigma_I/(I(Lp))^{-1/2}$, $\sigma_I = [\sigma_c^2 + (0.02N_{net})^2]^{1/2}$. Atomic scattering factors and programs used are those of ref 31 and 32.

Magnetic Properties

Qualitative Approach. The magnetic behavior of $MnCu(obp)(H_2O)_3 \cdot H_2O$ is represented in Figure 3, in the form of an $\chi_M T$ versus T plot, χ_M being the molar magnetic susceptibility per MnCu unit and T the temperature. At 290 K, $\chi_M T$ is equal to 4.47 cm^3 mol^{-1} K. When the system cools down from room

Table II. Atomic Parameters for $MnCu(obp)(H_2O)_3 \cdot H_2O$

atom	x	y	z	B_{eq} or B,[a] Å^2
Cu	−0.00542 (3)	0.24436 (3)	0.46240 (2)	0.576 (5)
Mn	0.25715 (4)	0.14548 (4)	−0.07135 (3)	0.605 (7)
O1	0.3318 (2)	0.2096 (2)	0.0673 (1)	0.77 (3)
O2	0.0226 (2)	0.1176 (2)	0.1348 (1)	0.70 (3)
O3	0.0939 (2)	0.3201 (2)	0.5566 (1)	0.76 (3)
O4	−0.1993 (2)	0.1718 (2)	0.6489 (2)	0.78 (3)
O5	0.2227 (2)	0.4931 (2)	0.5624 (2)	1.00 (3)
O6	−0.4781 (2)	0.1456 (2)	0.7847 (2)	1.23 (4)
O7	0.3105 (2)	−0.1187 (2)	0.0136 (2)	0.98 (3)
O8	0.1738 (2)	0.4043 (2)	−0.1526 (2)	1.15 (4)
O9	0.1322 (2)	0.1255 (2)	−0.1935 (2)	1.27 (4)
O10	0.2071 (2)	0.5926 (2)	−0.0146 (2)	1.32 (4)
N1	0.2060 (2)	0.2714 (2)	0.2856 (2)	0.71 (4)
N2	−0.0836 (2)	0.1662 (2)	0.3581 (2)	0.69 (4)
C1	0.0335 (3)	0.1617 (2)	0.2292 (2)	0.64 (4)
C2	0.2071 (3)	0.2192 (2)	0.1884 (2)	0.62 (4)
C3	0.3592 (3)	0.3367 (3)	0.2594 (2)	0.82 (4)
C4	0.3002 (3)	0.4703 (3)	0.3266 (2)	0.85 (5)
C5	0.2008 (3)	0.4252 (2)	0.4926 (2)	0.67 (4)
C6	−0.2543 (3)	0.1109 (3)	0.4164 (2)	0.73 (4)
C7	−0.3926 (3)	0.1919 (3)	0.5292 (2)	0.81 (5)
C8	−0.3541 (3)	0.1670 (2)	0.6620 (2)	0.67 (4)
H31	0.418 (3)	0.374 (3)	0.162 (2)	0.4 (5)*
H32	0.440 (3)	0.259 (3)	0.296 (2)	0.4 (5)*
H41	0.228 (3)	0.546 (3)	0.284 (2)	0.7 (5)*
H42	0.401 (3)	0.518 (3)	0.297 (2)	0.7 (5)*
H61	−0.246 (3)	−0.004 (3)	0.464 (2)	0.6 (5)*
H62	−0.296 (3)	0.134 (3)	0.341 (2)	0.7 (5)*
H71	−0.407 (3)	0.301 (3)	0.484 (2)	0.2 (5)*
H72	−0.503 (3)	0.157 (3)	0.558 (2)	1.1 (6)*
H73	0.277 (4)	−0.131 (3)	0.093 (3)	2.4 (7)*
H74	0.401 (4)	−0.143 (4)	−0.015 (3)	2.8 (7)*
H81	0.181 (4)	0.432 (3)	−0.227 (3)	2.6 (7)*
H82	0.206 (4)	0.452 (3)	−0.134 (3)	2.7 (7)*
H91	0.105 (3)	0.192 (3)	−0.259 (3)	1.8 (6)*
H92	0.098 (3)	0.054 (3)	−0.178 (3)	2.1 (7)*
H101	0.104 (4)	0.597 (3)	0.040 (3)	2.3 (7)*
H102	0.224 (4)	0.678 (4)	−0.037 (3)	3.2 (8)*

[a] B values marked with an asterisk denote isotropically refined atoms. Values fro anisotropically refined atoms are given in the form of the isotropic equivalent thermal parameter $B_{eq} = {}^4/_3 \sum_i \sum_j \beta_{ij} \mathbf{a}_i \cdot \mathbf{a}_j$.

Table III. Bond Distances (Å) Involving Non-Hydrogen Atoms in $MnCu(obp)(H_2O)_3 \cdot H_2O$[a]

Cu–O3	1.962 (2)	O3–C5	1.291 (3)
Cu–O4	1.947 (1)	O4–C8	1.277 (3)
Cu–O5[a]	2.625 (1)	O5–C5	1.238 (4)
Cu–N1	1.927 (1)	O6–C8	1.245 (2)
Cu–N2	1.938 (2)	N1–C2	1.296 (4)
Mn–O1	2.162 (2)	N1–C3	1.459 (3)
Mn–O2	2.195 (1)	N2–C1	1.297 (2)
Mn–O6[b]	2.085 (1)	N2–C6	1.458 (3)
Mn–O7	2.254 (2)	C1–C2	1.531 (3)
Mn–O8	2.244 (2)	C3–C4	1.517 (4)
Mn–O9	2.103 (2)	C4–C5	1.523 (3)
O1–C2	1.270 (2)	C6–C7	1.526 (3)
O2–C1	1.268 (3)	C7–C8	1.519 (4)

[a] Symmetry operations: (a) $-x$, $1-y$, $1-z$; (b) $1+x$, y, $z-1$.

temperature, $\chi_M T$ decreases in a rather smooth fashion and reaches a rounded minimum at about 40 K with $\chi_M T = 3.65$ cm^3 mol^{-1} K. Below 40 K, $\chi_M T$ increases more and more rapidly before reaching a sharp maximum at 2.9 K with $\chi_M T = 8.03$ cm^3 mol^{-1} K. Below 2.9 K, $\chi_M T$ quickly falls. The maximum of $\chi_M T$ at 2.9 K is associated with a maximum of χ_M at 2.31 (2) K with $\chi_M = 3.21$ cm^3 mol^{-1}. The temperature dependence of χ_M in the 1.5–4.5 K temperature range is shown in Figure 4.

Qualitatively, the interpretation of these magnetic properties is rather similar to that of the ordered bimetallic chains already described.[15-26] From a magnetic viewpoint, the compound consists of $Mn^{II}Cu^{II}$ alternating bimetallic chains. Indeed, the copper(II) ion is in square-pyramidal surroundings with a long apical bond (Cu^a–O5 = 2.625 Å). The unpaired electron around copper(II)

Table IV. Bond Angles Involving Non-Hydrogen Atoms in $MnCu(obp)(H_2O)_3 \cdot H_2O$

O3–Cu–O4	90.86 (7)	Cu–O3–C5	126.6 (2)
O3–Cu–O5[a]	90.19 (6)	Cu–O4–C8	124.4 (1)
O3–Cu–N1	91.54 (2)	Cu[a]–O5–C5	103.6 (1)
O3–Cu–N2	175.23 (6)	Mn[c]–O6–C8	154.9 (2)
O4–Cu–O5[a]	83.39 (2)	Cu–N1–C2	114.0 (2)
O4–Cu–N1	168.29 (2)	Cu–N1–C3	125.5 (2)
O4–Cu–N2	93.22 (7)	C2–N1–C3	120.4 (2)
O5[a]–Cu–N1	108.06 (6)	Cu–N2–C1	113.9 (2)
O5[a]–Cu–N2	92.72 (7)	Cu–N2–C6	125.9 (1)
N1–Cu–N2	83.97 (8)	C1–N2–C6	121.1 (2)
O1–Mn–O2	76.44 (6)	O2–C1–N2	129.0 (2)
O1–Mn–O6[b]	86.81 (7)	O2–C1–C2	117.1 (2)
O1–Mn–O7	99.10 (7)	N2–C1–C2	113.9 (2)
O1–Mn–O8	85.18 (7)	O1–C2–N1	128.5 (2)
O1–Mn–O9	166.03 (6)	O1–C2–C1	117.5 (2)
O2–Mn–O6[b]	159.99 (7)	N1–C2–C1	114.0 (2)
O2–Mn–O7	83.82 (5)	N1–C3–C4	110.2 (2)
O2–Mn–O8	92.43 (5)	C3–C4–C5	115.6 (2)
O2–Mn–O9	95.27 (6)	O3–C5–O5	121.7 (2)
O6[b]–Mn–O7	88.19 (6)	O3–C5–C4	119.7 (2)
O6[b]–Mn–O8	97.03 (6)	O5–C5–C4	118.7 (2)
O6[b]–Mn–O9	103.20 (7)	N2–C6–C7	110.4 (2)
O7–Mn–O8	173.45 (7)	C6–C7–C8	116.0 (2)
O7–Mn–O9	91.03 (7)	O4–C8–O6	120.1 (2)
O8–Mn–O9	83.95 (7)	O4–C8–C7	121.2 (2)
Mn–O1–C2	114.5 (2)	O6–C8–C7	118.7 (2)
Mn–O2–C1	113.9 (1)		

[a] Symmetry operations: (a) $-x$, $1-y$, $1-z$; (b) $1+x$, y, $z-1$; (c) $x-1$, y, $1+z$.

Table V. Hydrogen Bonds in $MnCu(obp)(H_2O)_3 \cdot H_2O$

A	D	A---D, Å	∠A---H–D, deg
O1	O7($1-x$, $-y$, $-z$)	2.748 (2)	170 (4)
O2	O9($-x$, $-y$, $-z$)	2.648 (3)	172 (3)
O3	O9(x, y, $1+z$)	2.701 (2)	165 (2)
O5	O8(x, y, $1+z$)	2.696 (2)	174 (3)
O6	O7($-x$, $-y$, $1-z$)	2.987 (3)	122 (3)
O8	O10($-x$, $1-y$, $-z$)	2.921 (2)	169 (4)
O10	O8(x, y, z)	2.808 (3)	159 (3)

is described by a xy-type magnetic orbital pointing from the metal toward the four nearest neighbor atoms, N1, N2, O3, and O4, in the equatorial plane. This magnetic orbital overlaps the xy-type magnetic orbital centered on manganese(II) through the oxamido bridge on the one hand and through the carboxylato bridge on the other hand, as schematized below. x and y refer to local axes along the bisectrices of the bond angles in the equatorial planes.

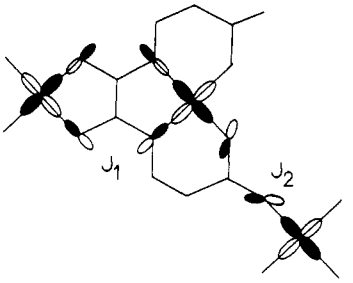

The former bridging network is well-known to favor an exceptionally strong antiferromagnetic interaction,[27] and the latter may be expected to give rise to a weaker antiferromagnetic one. This kind of single carboxylato bridge has been reported in the copper(II) chain compound $Cu(NH_3)_2(CH_3COO)Br$, in which an intrachain exchange parameter of -6 cm^{-1} has been found.[28] In contrast, the interaction between the symmetry-related copper(II) ions through the bridge O3C5O5 is certainly extremely weak. Indeed, the site symmetry of the copper(II) ion is very close to C_{2v}, and the xy-type magnetic orbital transforming as b_1 does not

(27) Kahn, O. *Angew. Chem., Int. Ed. Engl.* **1985**, *24*, 834.
(28) Carlin, R. L.; Kopinga, K.; Kahn, O.; Verdaguer, M. *Inorg. Chem.* **1986**, *25*, 1786.

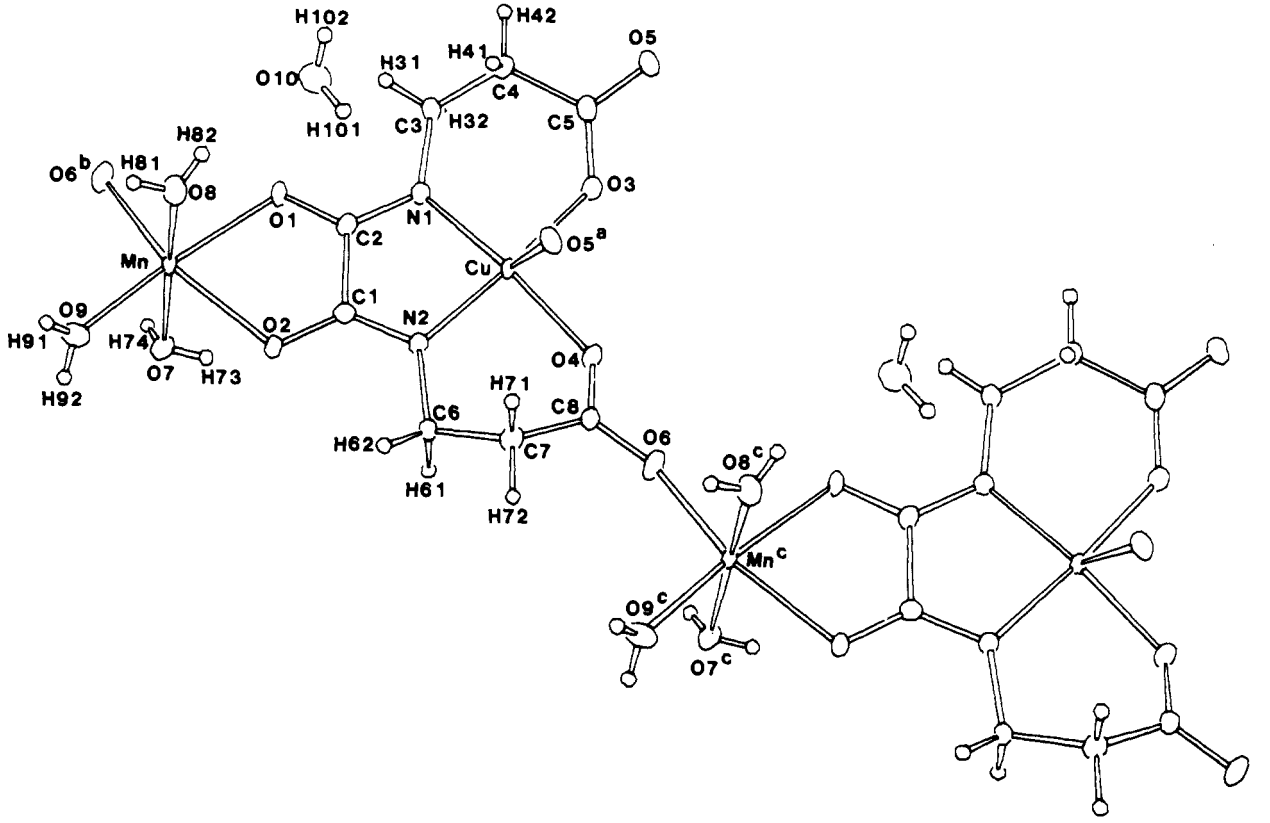

Figure 1. Section of single chain showing the atomic numbering used. Thermal ellipsoids of non-hydrogen atoms are plotted at the 70% probability level. Hydrogen atoms are given an arbitrary radius.

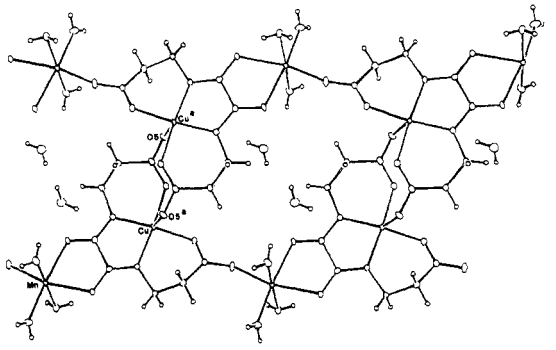

Figure 2. Section of a double chain.

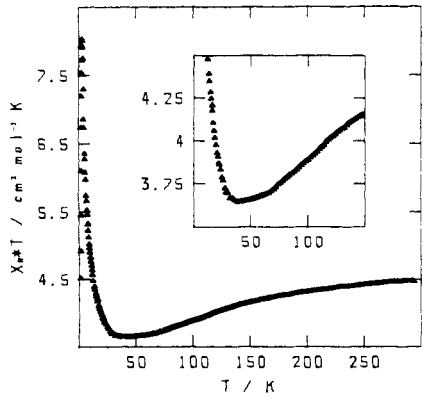

Figure 3. Temperature dependence of $\chi_M T$ for $MnCu(obp)(H_2O)_3 \cdot H_2O$.

mix at the first order with the z^2-type magnetic orbital transforming as a_1 and pointing toward the O5 apical site. In other words, the spin density delocalized from Cu^a to O5 is almost negligible as well as the overlap density in the O3C5O5 bridge.[29]

(29) Kahn, O. *Struct. Bonding (Berlin)*, in press.

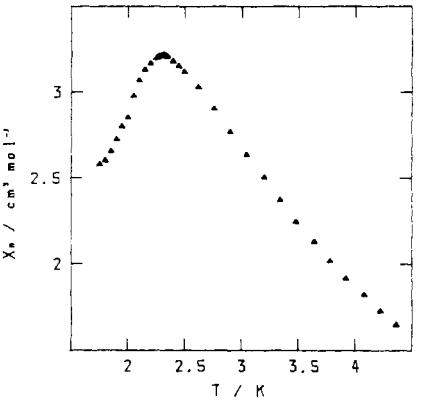

Figure 4. Temperature dependence of χ_M for $MnCu(obp)(H_2O)_3 \cdot H_2O$ in the 1.5–4.5 K temperature range.

To sum up, we are essentially faced with $Mn^{II}Cu^{II}$ alternating bimetallic chains with two intrachain interaction parameters J_1 through oxamido and J_2 through carboxylato. Weak interchain interactions may superimpose onto the dominant intrachain interactions, which will influence the magnetic data only in the low-temperature range. Ignoring these interchain effects, we can schematize the most excited state as

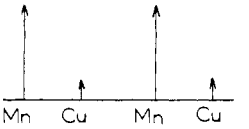

and the ground state as

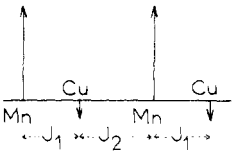

At high temperature ($kT \gg |J_1|$ and $|J_2|$), $\chi_M T$ is equal to the sum of what is expected for isolated Mn^{II} and Cu^{II} ions. Upon cooling down, the first state to be thermally depopulated is that of highest spin multiplicity, so that $\chi_M T$ decreases. On the other hand, in the low-temperature range, the system $(MnCu)_N$ becomes roughly similar to a chain of N local spins $S = 2$ ferromagnetically coupled, and $\chi_M T$ diverges when T approaches zero. It follows that $\chi_M T$ exhibits a minimum at a finite temperature. It is also possible to discuss qualitatively the position of this minimum versus the ratio $\rho = J_2/J_1$ with $0 \leq \rho \leq 1$. For $\rho = 0$, the system reduces to antiferromagnetically coupled $Mn^{II}Cu^{II}$ pairs without any interaction between these pairs, and $\chi_M T$ tends to the value $\chi_M T = 3.00(g^2/4)$ cm^3 mol^{-1} K corresponding to an isolated spin quintet state when T approaches zero.[30] In other words, the minimum of $\chi_M T$ occurs at 0 K. When ρ increases, a small ferromagnetic-like interaction appears between the $Mn^{II}Cu^{II}$ pairs coupled through J_1 and $\chi_M T$ exhibits a minimum at a nonzero temperature. The larger ρ is, the higher the $kT/|J_1|$ value of the minimum. For $\rho = 1$, the system becomes an equally spaced $Mn^{II}Cu^{II}$ bimetallic chain and the minimum of $\chi_M T$ has been found for $kT/|J_1| = 2.98$, for a model where the $S_{Mn} = {}^5/_2$ spin is taken as semiquantum and the $S_{Cu} = {}^1/_2$ spin as quantum.[23] In this model, the local g factors g_{Mn} and g_{Cu} are assumed to be equal and isotropic.

Experimentally, the divergence of $\chi_M T$ is stopped at 2.9 K. This is due to the onset of a three-dimensional antiferromagnetic ordering at 2.31 K. The alternating bimetallic chains are not perfectly isolated in the crystal lattice. They couple antiferromagnetically. The nature of the interchain interactions may be attributed to the fact that the shortest interchain metal···metal separations involve metal ions of the same kind[19] (Cu···Cu = 4.262 Å and Mn···Mn = 4.819 Å). If we assume that all the interactions between pairs of neighbor ions, within the chain as well as between the chains, are antiferromagnetic, then the relative positions of the chains favor an antiferromagnetic ordering:

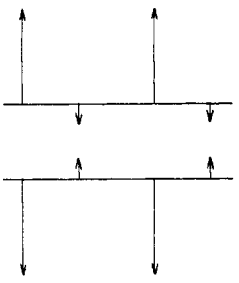

Quantitative Approach. We consider the Heisenberg chain Hamiltonian

$$H = \sum_i H_i \tag{1}$$

with

$$H_i = -J\vec{s}_i[(1 + \alpha)\vec{S}_i + (1 - \alpha)\vec{S}_{i+1}] \tag{2}$$

$\vec{s}_i$ refers to a spin vector with quantum number s, carrying the magnetic moment $g\vec{s}_i$, and $\vec{S}_i$ stands for a spin vector with a quantum number large enough to be treated classically. Thus $\vec{S}_i$ is considered as a unit vector and the corresponding magnetic moment is $G\vec{S}_i$. Each spin $\vec{s}_i$ is coupled through $J(1 + \alpha)$ and $J(1 - \alpha)$ with its nearest neighbors $\vec{S}_i$ and $\vec{S}_{i+1}$. In order to get the zero-field magnetic susceptibility of the chain, let us consider the various spin–spin correlations that are involved in the overall magnetic moment fluctuations. To begin with, we examine the chain running from $\vec{S}_i$ to $\vec{S}_j$ ($j > i$). The corresponding partition function is

$$Z_{i,j} = \int d\vec{S}_i \, \mathrm{Tr}_i \int d\vec{S}_{i+1} \, \mathrm{Tr}_{i+1} \cdots \int d\vec{S}_j \, \mathrm{Tr}_j \exp(-\beta \sum_{k=i}^{j-1} H_k) \tag{3}$$

β stands for $1/kT$, k being the Boltzmann constant. Here, $\int d\vec{S}_k$ means integrating over the angular coordinates of $\vec{S}_k$, and Tr_k summing over a complete set of orthogonal states of $\vec{s}_k$. Due to isotropic symmetry of H, we can write

$$\mathrm{Tr}_k \, [\exp(-\beta H_k)] = \sum_{l=0}^{\infty} \sum_{m=-l}^{l} A_l(\beta,J,\alpha) \, Y_l^{-m}(\vec{S}_k) \, Y_l^m(\vec{S}_{k+1}) \tag{4}$$

$Y_l^m(\vec{S}_k)$ is the spherical harmonic expressed in terms of the spherical coordinates of the $\vec{S}_k$ direction. As easily shown, $A_l(\beta,J,\alpha)$ is given by

$$A_l(\beta,J,\alpha) = 2\pi \sum_{\sigma=-s}^{+s} \int_{-1}^{+1} \exp[\sigma\lambda(1 + \eta u)^{1/2}] \, P_l(u) \, du \tag{5}$$

where $P_l(u)$ is the Legendre polynomial of degree l, and

$$\lambda = -\beta J[2(1 + \alpha^2)]^{1/2} \qquad \eta = (1 - \alpha^2)/(1 + \alpha^2) \tag{6}$$

Now, inserting (4)–(6) into (3) and integrating over the classical spin directions, we get

$$Z_{i,j} = 4\pi[A_0(\beta,J,\alpha)]^{j-i} \tag{7}$$

Let us specify the z direction in the spin space; it results from isotropy so that we have

$$\langle \vec{S}_i \cdot \vec{S}_j \rangle = 3\langle S_i^z S_j^z \rangle \tag{8}$$

and similar relations for the pairs $\vec{S}_i$, $\vec{s}_j$ and $\vec{s}_i$, $\vec{s}_j$. $\langle X \rangle$ means the ensemble average for the measurable X. Since we have

$$S^z = (4\pi/3)^{1/2} \, Y_1^0(\vec{S}) \tag{9}$$

we can write

$$\langle \vec{S}_i \cdot \vec{S}_j \rangle = (Z_{i,j})^{-1} \int d\vec{S}_i \, \mathrm{Tr}_i \cdots \int d\vec{S}_j \, Y_1^0(\vec{S}_i) \, Y_1^0(\vec{S}_j) \exp(-\beta \sum_{k=i}^{j-1} H_k) \tag{10}$$

This involves exactly the same sets of integrations and state summations as (4). Performing them, we get the simple result

$$\langle \vec{S}_i \cdot \vec{S}_j \rangle = [A_1(\beta,J,\alpha)/A_0(\beta,J,\alpha)]^{j-i} \tag{11}$$

Notice that for $i = j$, this reduces to unity, which is the convenient value.

We now turn to the calculation of $\langle s_i^z S_j^z \rangle$. For that, we need an intermediate reference axis system for $\vec{s}_i$, with the z' axis orientated along the local exchange field direction defined by $(1 + \alpha)\vec{S}_i + (1 - \alpha)\vec{S}_{i+1}$. Let $C(\vec{S}_i,\vec{S}_{i+1})$ represent the cosine of the angle between the z and z' directions. We have

$$C(\vec{S}_i,\vec{S}_{i+1}) = \frac{(1 + \alpha) \, Y_1^0(\vec{S}_i) + (1 - \alpha) \, Y_1^0(\vec{S}_{i+1})}{[2(1 + \alpha^2)]^{1/2}(1 + \eta \cos \theta_{i,i+1})^{1/2}} \tag{12}$$

where $\theta_{i,i+1}$ is the angle between $\vec{S}_i$ and $\vec{S}_{i+1}$. With this in mind, we obtain

$$\mathrm{Tr}_i \, [s_i^z \exp(-\beta H_i)] = \beta J(4\pi/3)^{1/2} \, [(1 + \alpha) \, Y_1^0(\vec{S}_i) + (1 - \alpha) Y_1^0(\vec{S}_{i+1})] \sum_{l=0}^{\infty} \sum_{m=-l}^{l} B_l(\beta,J,\alpha) \, Y_l^{-m}(\vec{S}_i) \, Y_l^m(\vec{S}_{i+1}) \tag{13}$$

with

$$B_l(\beta,J,\alpha) = 2\pi \sum_{\sigma=-s}^{s} \sigma^2 \int_{-1}^{+1} \frac{\exp[\sigma\lambda(1 + \eta u)]^{1/2}}{\sigma\lambda(1 + \eta u)^{1/2}} \, P_l(u) \, du \tag{14}$$

The correlation $\langle \vec{s}_i \cdot \vec{S}_j \rangle$ is then given by

$$\langle \vec{s}_i \cdot \vec{S}_j \rangle = (Z_{i,j})^{-1}(12\pi)^{1/2} \int d\vec{S}_i \, \mathrm{Tr}_i \cdots \int d\vec{S}_j \, s_i^z Y_1^0(\vec{S}_j) \exp(-\beta \sum_{k=i}^{j-1} H_k) \tag{15}$$

(30) Seiden, J. *J. Phys. Lett.* **1983**, *44*, L947.
(31) Cromer, D. T.; Waber, J. T. *International Tables for X-ray Crystallography*; Kynoch: Birmingham, England, 1974, Vol. IV, p 99 (Table 2.2.B).
(32) Frenz, B. A. *The SDP-User's Guide*; Enraf-Nonius: Delft, The Netherlands, 1983.

Summing and integrating leads to the result

$$\langle \vec{s}_i \cdot \vec{S}_j \rangle = \beta J[(1-\alpha)B_0 + (1+\alpha)B_1]A_1^{j-1-i}/A_0^{j-i} \quad (16)$$

A_l stands for $A_l(\beta,J,\alpha)$ and B_l for $B_l(\beta,J,\alpha)$. For $j \geq i$, a similar procedure gives $\langle \vec{S}_i \cdot \vec{s}_j \rangle$, which is obtained from (16) by changing α, $j-i-1$, and $j-i$ into $-\alpha$, $j-i$, and $j-i+1$, respectively. Now using expression 13 twice and performing the same type of calculation, we easily get, for $j > i$

$$\langle \vec{s}_i \cdot \vec{s}_j \rangle = (\beta J)^2[(1-\alpha)B_0 + (1+\alpha)B_1] \times [(1+\alpha)B_0 + (1-\alpha)B_1]A_1^{j-i-1}/A_0^{j-i} \quad (17)$$

It is now straightforward to calculate the fluctuations of the total magnetic moment $\vec{\mu}$ of the chain that runs from S_i to S_j ($j > i$), in units of μ_B:

$$\langle \vec{\mu}^2 \rangle = g^2 \sum_{k=i}^{j-1} \sum_{l=i}^{j-1} \langle \vec{s}_k \cdot \vec{s}_l \rangle + 2gG \sum_{k=i}^{j-1} \sum_{l=i}^{j} \langle \vec{s}_k \cdot \vec{S}_l \rangle + G^2 \sum_{k=i}^{j} \sum_{l=i}^{j} \langle \vec{S}_k \cdot \vec{S}_l \rangle \quad (18)$$

Using the well-known expression for the magnetic susceptibility χ referred to the bimetallic unit cell

$$\chi = \beta/3\langle \vec{\mu}^2 \rangle \quad (19)$$

and introducing the various correlations into (18), we obtain for the molar magnetic susceptibility per MnCu unit

$$\chi_M = (N\mu_B^2\beta/3)\{q^2[s(s+1) \times (1-P) + 2RQ] + 2gG(R+Q) + G^2(1+P)\}/(1-P) \quad (20)$$

where P, Q, and R are defined as

$$P = A_1/A_0$$
$$Q = \beta J[(1+\alpha)B_0 + (1-\alpha)B_1]/A_0 \quad (21)$$
$$R = \beta J[(1-\alpha)B_0 + (1+\alpha)B_1]/A_0$$

So, only A_0, A_1, B_0 and B_1 have to be expressed versus β, J, and α. This is a straightforward work, leading to

$$A_0 = \frac{2\pi}{\Lambda^2} \sum_{\sigma=-s}^{+s} \sum_{\epsilon=\pm} \frac{\epsilon \exp(\sigma\lambda_\epsilon)}{\sigma^2}(\sigma\lambda_\epsilon - 1)$$

$$A_1 = \frac{\pi}{2\Lambda^2} \sum_{\sigma=-s}^{+s} \sum_{\epsilon=\pm} \frac{\epsilon \exp(\sigma\lambda_\epsilon)}{\sigma^4} \left[\frac{1-\alpha^2}{2}(\sigma\lambda_\epsilon)^3 + \frac{\alpha^2-5}{2}(\sigma\lambda_\epsilon)^2 + 6(\sigma\lambda_\epsilon - 1) \right]$$

$$B_0 = \frac{2\pi}{\Lambda^2} \sum_{\sigma=-s}^{+s} \sum_{\epsilon=\pm} \epsilon \exp(\sigma\lambda_\epsilon)$$

$$B_1 = \frac{\pi}{2\Lambda^2} \sum_{\sigma=-s}^{+s} \sum_{\epsilon=\pm} \frac{\epsilon \exp(\sigma\lambda_\epsilon)}{\sigma^2} \left[\frac{1-\alpha^2}{2}(\sigma\lambda_\epsilon)^2 - 2\sigma\lambda_\epsilon + 2 \right] \quad (22)$$

with

$$\lambda_+ = -2\beta J \qquad \lambda_- = \alpha\lambda_+ \qquad \Lambda^2 = (1-\alpha^2)\beta^2J^2 \quad (23)$$

If we let α vanish and s take the value $^1/_2$, expressions 20–22 reduce to the result derived by Seiden, who considered the case of $Mn^{II}Cu^{II}$ uniform bimetallic chains with $S_{Cu} = {}^1/_2$ and S_{Mn} being a classical spin.[30]

We have fitted the experimental data down to 10 K with the theoretical expressions 20–22, using $s = {}^1/_2$ and letting J, G, g, and α vary. The best agreement was obtained for

$$J_1 = (1+\alpha)J = (-46 \pm 1)K = -32 \pm 0.7 \text{ cm}^{-1}$$
$$J_2 = (1-\alpha)J = (-9.8 \pm 1)K = -6.8 \pm 0.7 \text{ cm}^{-1}$$
$$G = 5.02 \qquad g = 2.32$$

We will discuss the values of the interaction parameters $(1 \pm \alpha)J$ in the next section. As far as the G and g values are concerned, $G = 5.02$ corresponds well to what is expected for $g_{Mn}S_{Mn}$. On the other hand, the $g = 2.32$ value appears slightly too large for the g factor of a Cu^{II} ion in square-pyramidal surroundings.

Discussion

In this paper, we describe the first alternating bimetallic chain compound. In fact, structurally the system consists of centrosymmetrically related double chains, but the interaction between two symmetry-related Cu^{II} ions through a long Cu–O apical bond is expected to be negligible as compared to the interactions between Mn^{II} and Cu^{II} ions within a single chain through an oxamido and a carboxylato bridge, respectively. In the 3–300 K temperature range, the compound qualitatively exhibits the magnetic behavior characteristic of antiferromagnetically coupled bimetallic chains with a minimum in the $\chi_M T$ versus T plot and a divergence upon cooling down. The minimum occurs at 40 K, i.e. much lower than it would be expected for a regular bimetallic chain with only oxamido bridges. This is due to the fact that the carboxylato bridge is less efficient than the oxamido bridge in propagating the interaction. For an oxamido-bridged $Mn^{II}Cu^{II}$ regular chain, the minimum of $\chi_M T$ would occur in the 110–140 K range.[15,18-20] The increase of $\chi_M T$ upon cooling down below 40 K is due to the augmentation of the correlation length between antiferromagnetically coupled pairs of $S_{Mn} = {}^5/_2$ and $S_{Cu} = {}^1/_2$ local spins within the chain. For a given temperature, this correlation length is however smaller than in the $Mn^{II}Cu^{II}$ chain compounds already described with dithiooxalato or oxamato bridges.[1,18-20] For instance, both the title compound and $MnCu(pba)(H_2O)_3 \cdot 2H_2O$ exhibit a three-dimensional antiferromagnetic ordering around 2.3 K.[19] Just above the antiferromagnetic transition temperature, $\chi_M T$ presents a sharp maximum. The value of this maximum is 8.03 cm^3 mol^{-1} K for the title compound and 20.9 cm^3 mol^{-1} K for $MnCu(pba)(H_2O)_3 \cdot 2H_2O$.

The antiferromagnetic nature of the long-range order in $MnCu(obp)(H_2O)_3 \cdot H_2O$ is attributed to the fact that between the symmetry-related chains as well as between neighboring double chains, the shortest metal···metal separations are Cu···Cu and Mn···Mn and not Cu···Mn. The same situation has been found in the regular chains $MnCu(dto)(H_2O)_3 \cdot 4.5H_2O$[15] and $MnCu(pba)(H_2O)_3 \cdot 2H_2O$.[19] In contrast, in $MnCu(pbaOH)(H_2O)_3$, the shortest interchain metal···metal distance along one of the directions perpendicular to the chain axis is Cu···Mn and the compound orders ferromagnetically. In principle, it might be possible with alternating as well as with regular bimetallic chains to modify the relative positions of the chains in such a way as to avoid the compensation of the local spins and to obtain a resulting magnetic moment. We are currently exploring several synthesis routes along this line.

The synthesis of this new kind of one-dimensional magnet pushed us to develop a theoretical formalism to interpret quantitatively the magnetic data. The two key approximations of this formalism are as follows: (i) the interaction between Mn^{II} and Cu^{II} ions is purely isotropic; (ii) the S_{Mn} local spins are large enough to be treated classically. The theoretical expressions for the magnetic susceptibility valid for any alternating bimetallic chain with the classical–quantum alternation are given and applied to the specific case where the quantum spin is $^1/_2$. The interaction parameter through the oxamido bridge is found to be equal to -32 cm^{-1}. This value is larger than that found in the $Mn^{II}Cu^{II}$ systems with oxamato bridges (-24 cm^{-1}). This confirms, if it was still necessary, that the replacement of an oxygen atom by a nitrogen atom in the bridging network increases the magnitude of the interaction, owing to the larger delocalization of the magnetic orbital centered on Cu^{II}. The interaction parameter through the carboxylato bridge is found to be equal to -6.8 cm^{-1}. The ratio of the two parameters $[J_1/J_2 = (1+\alpha)/(1-\alpha)]$ is equal to 4.7. It is quite remarkable that this ratio is rather close to 4. Indeed, it has been established that the magnitude of the antiferromagnetic interaction varies as the square of the overlap integral between interacting magnetic orbitals. The two xy-type magnetic orbitals overlap on either side of the bridge through the oxamido group but only on one side through the carboxylato group (see the drawing of the orbital pathways above), so that one could

well expect the overlap integrals to be in a ratio close to 2.

To conclude, we will point out that the design of the alternating bimetallic chain described in this paper represents a significant step in the field of the low-dimensional magnetism. We are looking for novel systems in which the spin order would be even more subtle.

Registry No. $MnCu(obp)(H_2O)_3 \cdot H_2O$, 111436-56-7; diethyl oxalate, 95-92-1; β-alanine, 107-95-9.

Supplementary Material Available: Table SI, listing the anisotropic thermal parameters (1 page); a table of calculated and observed structure factors (10 pages). Ordering information is given on any current masthead page.

Contribution from the Department of Chemistry,
Iowa State University, Ames, Iowa 50011

Zirconium Iodide Clusters That Encapsulate Silicon, Germanium, Phosphorus, or Pyrex

Guy Rosenthal and John D. Corbett*

Received August 21, 1987

The phases $Zr_6I_{14}Z$ (Z = Si, Ge, P) as well as $M_xZr_6I_{14}P$ (M = Cs, Rb) have been synthesized by reaction of stoichiometric amounts of ZrI_4, Z (as the element), M^I when appropriate, and excess Zr in sealed Ta containers at 700–850 °C. Experiments with a longer list of main-group elements from the third and fourth periods as the potential interstitial Z gave only negative results as far as the formation of either the corresponding ternary or quaternary phase. The structure of $Cs_{0.35(1)}Zr_6I_{14}P$ was established by single-crystal X-ray diffraction (space group *Cmca*, Nb_6Cl_{14} type; a = 15.934 (1), b = 14.287 (1), c = 12.939 (1) Å; R = 0.050, R_w = 0.064 for 1428 reflections with $2\theta \leq 55°$). Distortions and bonding within the cluster are described. Some of the problems associated with adventitious impurities and mixed interstitials are also considered. The silicon and boron from a few percent of Pyrex glass impurity produce a moderate yield of well-crystallized $Cs_{0.54}Zr_6I_{14}(B,Si)$ (plus ZrO_2); the structural refinement and the dimensions of the cluster indicate about a 50:50 mixture of the two elements is encapsulated.

Introduction

An unprecedented variety of metal cluster halide phases of the early transition metals has recently been obtained through the bonding of an additional heteroelement in the center of the metal octahedra. Although the first examples[1] of these interstitially stabilized clusters arose via adventitious impurities, namely as what are now known to be $Zr_6Cl_{15}N$, $Sc_7Cl_{12}C$, and $Zr_6I_{12}C$,[2-4] our explorations demonstrate that a considerable number of other interstitial atoms may also be encapsulated. Variations of not only the interstitial element (Z) but also the oxidation state of the M_6X_{12}-type clusters through the addition of halide at terminal positions, countercations to the cluster framework, or both allow the preparation of a wide range of structural types and compositions.[5]

Although the greatest variety of structures presently known, eight all told, involve $Zr_6Cl_{12}Z$-type clusters in which chlorine bridges edges of the octahedron, these have been largely limited to examples containing interstitial Z = H, Be, B, C, or N.[2,5,6] On the other hand, the analogous zirconium iodide clusters appear to allow the inclusion of a greater range of interstitial elements, but to date only the $Zr_6I_{12}Z$ or $Zr_6I_{14}Z$ compositions and structures plus the alkali-metal derivatives of the second have been identified. In these cases, Z may be not only K, Al, or Si[7,8] but also Cr, Mn, Fe, or Co as in recently discovered examples.[9,10] Zirconium chloride and bromide clusters containing iron are now also known.[11]

Table I. Data Collection and Refinement Parameters for $Cs_{0.35}Zr_6I_{14}P$

space group	*Cmca*
Z	4
cryst dimens, mm	0.20 × 0.15 × 0.15
2θ(max), deg; octants	55; hkl, $\bar{h}kl$
no of reflcns: measd, obsd,[a] indep	3850, 2692, 1428
R(av), %	2.8
abs coeff μ, cm^{-1} (Mo Kα)	180
range of transm coeff (normalized)	0.62–1.0
sec ext coeff (10^{-7})	0.6 (1)
R,[b] %	5.0
R_w,[c] %	6.4

[a] $F_o \geq 3\sigma_F$ and $I_o > 3\sigma_I$. [b] $R = \sum(|F_o| - |F_c|)/\sum|F_o|$. [c] $R_w = [\sum w(|F_o| - |F_c|)^2/\sum w|F_o|^2]^{1/2}$.

Exploration of the range of main-group elements that may be so encapsulated in the iodides has now been extended to other third- and fourth-period elements. This paper reports on the formation of several cluster phases containing germanium or phosphorus and on a new silicon composition as well as on a longer list of main-group elements for which incorporation in a zirconium iodide cluster has not been successful. The considerable driving force associated with the formation of this type of compounds is also revealed by the preparation of a mixed silicon–boron example when Pyrex glass is the source of the interstitial elements.

Experimental Section

Syntheses. The purity, preparation, and handling of reactor grade Zr and ZrI_4 have been described.[12] Reagent grade CsI, RbI, and KI were vacuum sublimed prior to use. Red P (J. T. Baker) and zone-refined Si and Ge were employed as interstitial sources. All reactions were run in sealed Ta tubes with the aid of techniques described previously.[13] Stoichiometric amounts of ZrI_4, elemental Z, and, where appropriate, CsI, RbI, or KI were generally utilized together with about a 12-fold

(1) Corbett, J. D.; Daake, R. L.; Poeppelmeier, K. R.; Guthrie, D. H. *J. Am. Chem. Soc.* **1978**, *100*, 652.
(2) Ziebarth, R. P.; Corbett, J. D. *J. Less-Common Met.*, in press.
(3) Hwu, S.-J.; Corbett, J. D. *J. Solid State Chem.* **1986**, *64*, 331.
(4) Smith, J. D.; Corbett, J. D. *J. Am. Chem. Soc.* **1985**, *107*, 5704.
(5) Ziebarth, R. P.; Corbett, J. D. *J. Am. Chem. Soc.* **1985**, *107*, 4571.
(6) Ziebarth, R. P.; Corbett, J. D. *J. Am. Chem. Soc.* **1987**, *109*, 4844.
(7) Smith, J. D.; Corbett, J. D. *J. Am. Chem. Soc.* **1984**, *106*, 4618.
(8) Smith, J. D.; Corbett, J. D. *J. Am. Chem. Soc.* **1986**, *108*, 1927.
(9) Hughbanks, T.; Rosenthal, G.; Corbett, J. D. *J. Am. Chem. Soc.* **1986**, *108*, 8289.
(10) Hughbanks, T.; Rosenthal, G.; Corbett, J. D. *J. Am. Chem. Soc.*, in press.
(11) Zhang, J.; Ziebarth, R. P.; Hughbanks, T.; Corbett, J. D., unpublished research.
(12) Guthrie, D. H.; Corbett, J. D. *J. Solid State Chem.* **1981**, *37*, 256.
(13) Hwu, S.-J.; Corbett, J. D.; Poeppelmeier, K. R. *J. Solid State Chem.* **1985**, *57*, 43.

0020-1669/88/1327-0053$01.50/0 © 1988 American Chemical Society